Sea Surface Temperatures in the Indian Sub-Antarctic Southern Ocean for the Last Four Interglacial Periods

Sunil Kumar Shukla, Xavier Crosta, Minoru Ikehara

Geophysical Research Letters

RESEARCH LETTER
10.1029/2020GL090994

Key Points:

- First high-resolution sea-surface temperature (SST) record in the western Indian Southern Ocean over the past four interglacial periods (IG)
- Warmer Marine Isotope Stage 5e than 9e, 7e, and Holocene due to a combination of insolation, CO_2, and ocean-cryosphere interactions
- Stronger millennial variability in IG beyond the Holocene is mainly attributed to ocean circulation

Supporting Information:

Supporting Information may be found in the online version of this article.

Correspondence to:

S. K. Shukla,
sunilk_shukla@bsip.res.in

Citation:

Shukla, S. K., Crosta, X., & Ikehara, M. (2021). Sea surface temperatures in the Indian Sub-Antarctic Southern Ocean for the last four interglacial periods. *Geophysical Research Letters*, *48*, e2020GL090994. https://doi.org/10.1029/2020GL090994

Received 25 SEP 2020
Accepted 1 APR 2021

Sea Surface Temperatures in the Indian Sub-Antarctic Southern Ocean for the Last Four Interglacial Periods

Sunil Kumar Shukla[1], Xavier Crosta[2], and Minoru Ikehara[3]

[1]Birbal Sahni Institute of Palaeosciences, Lucknow, India, [2]Université de Bordeaux, CNRS, EPHE, Pessac Cedex, France, [3]Center for Advanced Marine Core Research, Kochi University, Kochi, Japan

Abstract Interglacial periods (IG) offer an opportunity to understand natural climate variability and its drivers under potential warmer-than-present conditions. However, sea-surface temperature (SST) records from the Southern Ocean (SO) are limited. The first SST record from the Sub-Antarctic western Indian SO covering the last four IGs suggest warmer conditions during Marine Isotope Stage 5e than 9e, 7e, and Holocene. Each IG presents two (early and late) warm phases interrupted by a cooling, except Holocene that experienced a continuous warming. The early warm phase might be attributable to changes in northern summer insolation with feedbacks from Northern and Southern Hemisphere ice-sheets, global oceanic circulation, and the carbon cycle. Conversely, the late warm phase might be due to changes in Southern Hemisphere summer insolation. Larger millennial-scale SST variability for IGs older than Holocene could be attributed to a less stable thermohaline circulation, which resulted in more variable heat redistribution between the two hemispheres.

Plain Language Summary Documenting the causes and consequences of climate variability during past warmer-than-present periods is essential to provide benchmarks to scenarios of future, projected climate variability. It is especially true for the Southern Ocean (SO) region, where the atmosphere, ocean, sea ice, cryosphere, and carbon cycle interact non-linearly at different timescales. We here provide the first high-resolution surface ocean temperature record covering the last four interglacial periods (IG) from the sub-Antarctic region of the western Indian sector of the SO. Our new results confirm that the atmospheric CO_2 concentrations and oceanic heat transport redistribution are important drivers for past IGs as suggested previously. These drivers are supplemented, during an interglacial early and late warmer phases, by Northern and Southern Hemisphere summer insolation, respectively. Our new results also show that millennial-scale variations in surface ocean temperature were much larger during IGs older than the Holocene, which we attribute to more variable thermohaline circulation, and subsequent heat transport to the SO, in older IGs. Our results suggest that variable thermohaline circulation is an intrinsic feature of warm climate states and question its stability over the coming centuries.

1. Introduction

The Southern Ocean (SO) is an important oceanic hub for redistributing heat, freshwater, carbon, and nutrients around the planet via the large-scale global oceanic circulation and hence plays a key part in the climate system (Marshall & Speer, 2012; Rintoul, 2018). The SO also absorbs a significant proportion of anthropogenic carbon emissions (Bushinsky et al., 2019; Le Quéré et al., 2018) and delivers heat that participates in the melting of ice shelves (Rignot et al., 2019). In return, glacial meltwater impacts on Antarctic sea-ice extent (Bintanja et al., 2013; Pauling et al., 2017) and the Atlantic Meridional Overturning Circulation (AMOC) by altering the upper and lower SO overturning cells (Bakker et al., 2017; Shin et al., 2003). As such, climate and oceanographic changes in the SO have global repercussions. Projections of SO climate changes over the next century include atmospheric and oceanic warming (Timmermann & Hellmer, 2013), sea-ice retreat (Lefebvre & Goosse, 2008), increase in ice-sheet melting (Golledge et al., 2015) and the slowdown of the AMOC (Rahmstorf et al., 2015) although feedbacks internal to the SO may delay such responses (Doddridge et al., 2019; Swingedouw et al., 2008). However, historical and instrumental data that feed climate models are too short for capturing the full range of natural climate variability and its drivers and forcing (Jones et al., 2016).

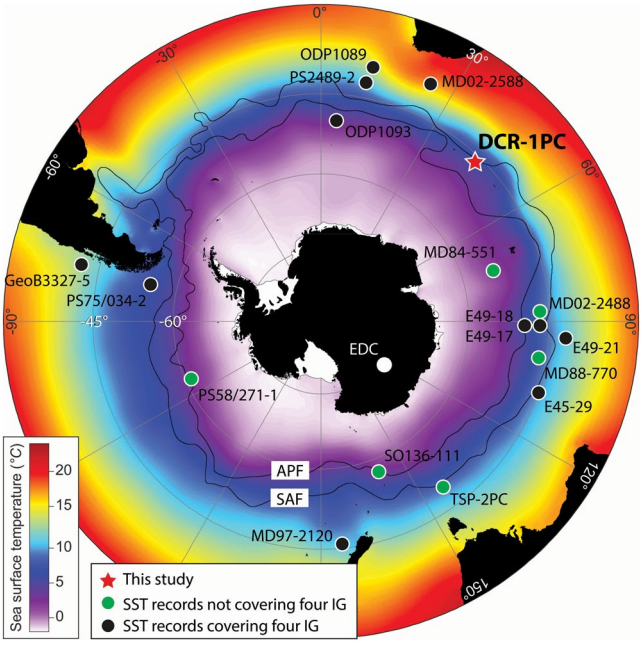

Figure 1. Locations of studied and discussed cores with the background map showing annual mean sea-surface temperature (SST) from the World Ocean Atlas 2013 (Locarnini et al., 2013). New SST data of DCR-1PC (red star) is compared with published SST records covering the past four interglacials (black circles–Becquey & Gersonde, 2003; Cortese et al., 2007; Ho et al., 2012; Howard & Prell, 1992; Pahnke et al., 2003; Romero et al., 2015; and Schneider-Mor et al., 2008) and EDC air temperature (white circle–Bazin et al., 2013). Records covering the past two interglacials are also shown (green circles - Crosta et al., 2004; Esper & Gersonde, 2014; Govin et al., 2009; Hays et al., 1976; Ikehara et al., 1997; Labeyrie et al., 1996; Pichon et al., 1992; and Waelbroeck et al., 1995). APF: Antarctic Polar Front; SAF: Sub-Antarctic Front (Orsi et al., 1995).

Past interglacial periods (IG) offer a window on climate variability under natural, sometimes warmer-than-present, conditions. The investigation of IG, particularly those occurring post the Mid-Brunhes Event (last 430 ka) when the one hundred thousand years cyclicity became established (Lisiecki & Raymo, 2005), is, therefore, crucial to understand the forcing and feedback processes under different insolation configurations. However, sea-surface temperature (SST) records covering several past IGs were mainly obtained from the Atlantic (Becquey & Gersonde, 2003; Cortese et al., 2007; Martínez-Garcia et al., 2009; Romero et al., 2015; Schneider-Mor et al., 2008), Pacific (Crosta et al., 2004; Ho et al., 2012; Ikehara et al., 1997; Pahnke et al., 2003), and southeastern Indian (Howard & Prell, 1992) sectors of the SO. Conversely, SST records from the Indian sector do not go beyond the last IG (Govin et al., 2009; Hays et al., 1976; Labeyrie et al., 1996; Pichon et al., 1992; Waelbroeck et al., 1995).

Previous studies have generally related the strength (i.e., the local mean SST expression) and length of past IGs in the SO to insolation changes at high northern latitudes with feedbacks from the Northern Hemisphere (NH) ice-sheet melting onto the AMOC and the meridional atmospheric circulation, both modulating the amount of heat delivered to the SO (e.g., Cortese et al., 2007; Martínez-Garcia et al., 2009). However, other feedback mechanisms such as atmospheric CO_2 changes (Past Interglacials Working Group of PAGES, 2016; hereafter PIWG, 2016; Yin, 2013) or Antarctic ice-sheet retreat (Holden et al., 2010) are essential to explain the strength of past IG. Additionally, as the temporal resolution of most SST records from the SO is relatively low (resolution ranges between ~500 and ~6,000 years), very little information on millennial climate variability and its potential drivers, within each IG, is available beyond the penultimate IG (Capron et al., 2014). We here provide a new diatom-based high-resolution (~190–675 years) SST record from the Sub-Antarctic western Indian sector of the SO covering the last four IGs. Our study aims to answer key questions, such as: (a) which IG was the warmest? (b) what climate variability was observable during each IG? and (c) what were the potential drivers of SO SST over the past four IGs?

2. Materials and Methods

The 10.2-m-long piston core DCR-1PC was collected during the expedition Hakuho-maru KH-10-7 in the austral summer 2010–2011, from Del Caño Rise (46°01.34′S – 44°15.24′E, 2632 m water depth) in the southwestern Indian sector of the SO (Figure 1). The core lies within the Antarctic Circumpolar Current that flows eastward between ~40°S and ~65°S in this region (Sokolov & Rintoul, 2009). The presence of several bathymetric highs and islands affects the mean zonal flow that is deflected northward in between Del Caño Rise and Crozet Plateau before turning again eastward (Pollard et al., 2007). Consequently, the core is situated below the modern Sub-Antarctic Front (SAF), where modern summer SST is ~7.5°C (Locarnini et al., 2013).

The age model for the top 80.43 cm of core DCR-1PC is based on seven radiocarbon dates obtained using mono-specific samples of planktic foraminifera species *Globigerina bulloides* and *Neogloboquadrina pachyderma* sinistral. Beyond this age, the core chronology was developed by tuning its SST record to EPICA Dome C deuterium record (Bazin et al., 2013; Jouzel et al., 2007). More details on DCR-1PC core chronology can be found in Crosta et al. (2020).

Diatoms extraction from the sediment samples and slide preparations were performed using the method described in Crosta et al. (2020). A total of 501 samples representing the last 350 ka were analyzed for their diatom content using the diatom counting technique detailed in Crosta and Koç (2007).

We applied the Modern Analog Technique (MAT) to the counted fossil diatoms for estimating the summer (January to March) SST. The method used 249 modern analogs, 33 diatom species and calculated SSTs based on 5 most similar analogs. This procedure resulted in a correlation coefficient of 0.96 and a root mean square error of prediction of 0.96°C on the validation step. More details can be found in Crosta et al. (2020).

3. Results and Discussion

3.1. DCR-1PC Sea-Surface Temperatures

The reconstructed SST over the past 350 ka from the sub-Antarctic western Indian SO shows a glacial-interglacial pattern with SST of ~4°C during the glacial periods and ~8°C during the IGs (Crosta et al., 2020) in agreement with SST reconstructions from the Atlantic sub-Antarctic zone (SAZ) (e.g., Martínez-Garcia et al., 2009). However, the reconstructed SST data suggest different climate conditions for the last four IGs, both in pattern and millennial-scale variability (Figure 2e).

In core DCR-1PC, the mean SST were 6.7°C (2.8–9.9°C) during MIS 9e, 7.7°C (5–10°C) during MIS 7e, 8.3°C (5.8–9.9°C) during MIS 5e and 7.6°C (5.3–9°C) during the Holocene (Figure 2e, Data Set SI-S01). Statistical analyses suggest that MIS 5e mean SST is significantly different than mean SSTs of other IGs, whereas mean SSTs of other IGs are non-significantly different among themselves (Tables S1-S6 in supporting information SI-S01). Therefore, past IG in core DCR-1PC can be ranked as a warmer MIS 5e and almost similarly warmer 9e, 7e, and Holocene.

In core DCR-1PC, the multi-millennial patterns of SST appear relatively different between the last four IGs. The three oldest IGs experienced two warm phases interrupted by a cooling phase. However, these phases' timing and amplitudes are quite different. During MIS 9e, the three phases are almost of the same duration (4–5 ka), and the early MIS 9e (338–334 ka) is cooler than the late MIS 9e (330–325 ka). Conversely, higher SST are reconstructed for the early MIS 7e, which appears much longer (247–240 ka) than the cooler late MIS 7e (237–234 ka). During the MIS 5e, the highest SST was also observed during the early part of IG. However, the first warm phase (131–127 ka) appears shorter than the second one (125–117 ka). Finally, the Holocene experienced a continuous warming from the early Holocene until the late Holocene (Figure S1 and Tables S7–S12 in supporting information SI-S01).

Millennial-scale SST variability, with different amplitudes for each IG, is superimposed onto the multi-millennial patterns. The largest SST amplitude of ~3.6°C was found during MIS 9e, whereas the smallest SST amplitude of ~1.8°C was observed during the Holocene. Both MIS 5e and 7e experienced intermediate SST amplitudes of ~2°C, and ~2.5°C, respectively (Figure 2e).

3.2. Southern Ocean Sea-Surface Temperatures

Comparison of our new SST data with published SO SST records allows obtaining a comprehensive picture of SST changes in terms of the strength of each IG along with their multi-millennial and millennial variability on a north-south transect over the last 350 ka (Figures 2 and 3). The SO SST records are based on different approaches, each bearing its own biases that are evaluated in Capron et al. (2014) and further discussed in supporting information SI-S01.

As expected, IGs mean SST are dictated by the cores' position relative to the mean hydrological features. The two cores from the Atlantic Subtropical Front (STF), MD02-2588 and ODP1089, present the highest mean SST of 19.7°C and 16.1°C, respectively, averaged over the past four IGs (Figures 3a and 3b). Higher mean SST during past IGs in core MD02-2588 may indicate the particularly strong Agulhas Current influence, bringing warmth from the low latitudes (Romero et al., 2015). Cores at 43–45°S from the northern SAZ off New-Zealand, MD97-2120, and in the mid-Atlantic, PS2489-2, present mean SST of 13.5°C and 10.2°C, respectively (Figures 3c and 3d). Although from similar latitude, core DCR-1PC is located at the modern SAF and presents a lower mean SST of 7.6°C during past IGs (Figure 3e). Finally, Antarctic Polar Front (APF) core ODP1093 presents a mean SST of 4°C (Figure 3f).

In core DCR-1PC, past IG can be ranked, from warmest to coldest, as MIS 5e, and almost similarly warm MIS 9e, 7e, and Holocene. Mean SST in MIS 5e appears significantly higher than in other IGs, whose means

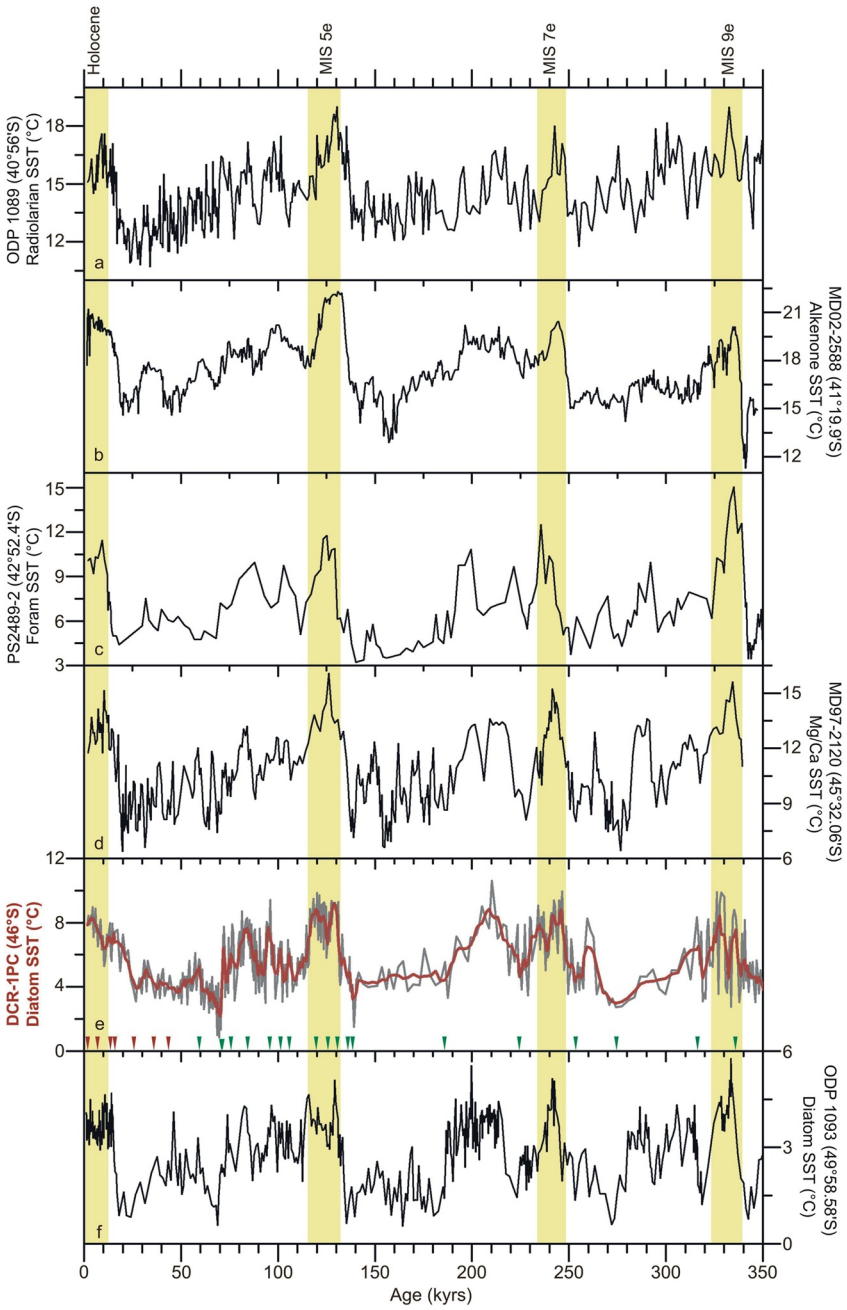

Figure 2. Diatom-based sea-surface temperature (SST) of DCR-1PC core for the past 350 ka with the different interglacial periods highlighted in yellow. The gray curve shows the original SST data, whereas red curve shows SST data smoothed with a 5-point moving average. Age control points along the bottom axis follow ^{14}C AMS dates (red triangles) and tie-points (Crosta et al., 2020) tuned with EPICA Dome C deuterium record. The DCR-1PC SST is compared with ODP Site 1089 from the subtropical Atlantic (Cortese et al., 2007), MD02-2588 core from the Agulhas Plateau (Romero et al., 2015), PS2489-2 core from the sub-Antarctic Atlantic (Becquey & Gersonde, 2003), MD97-2120 core from the sub-Antarctic Pacific (Pahnke et al., 2003), and ODP Site 1093 from the Atlantic Antarctic Polar Front (Schneider-Mor et al., 2008).

are instead not significantly different among themselves (Figure 3e). The MIS 5e is also the warmest in SAZ records presented here, even though it does not stand out in core MD97-2120 (Figure 3). The MIS 5e is also very warm interglacial in Pacific cores off South America (Ho et al., 2012) and Indian sector cores (Govin et al., 2009; Waelbroeck et al., 1995). Generally, MIS 7e and the Holocene experienced similar mean SST,

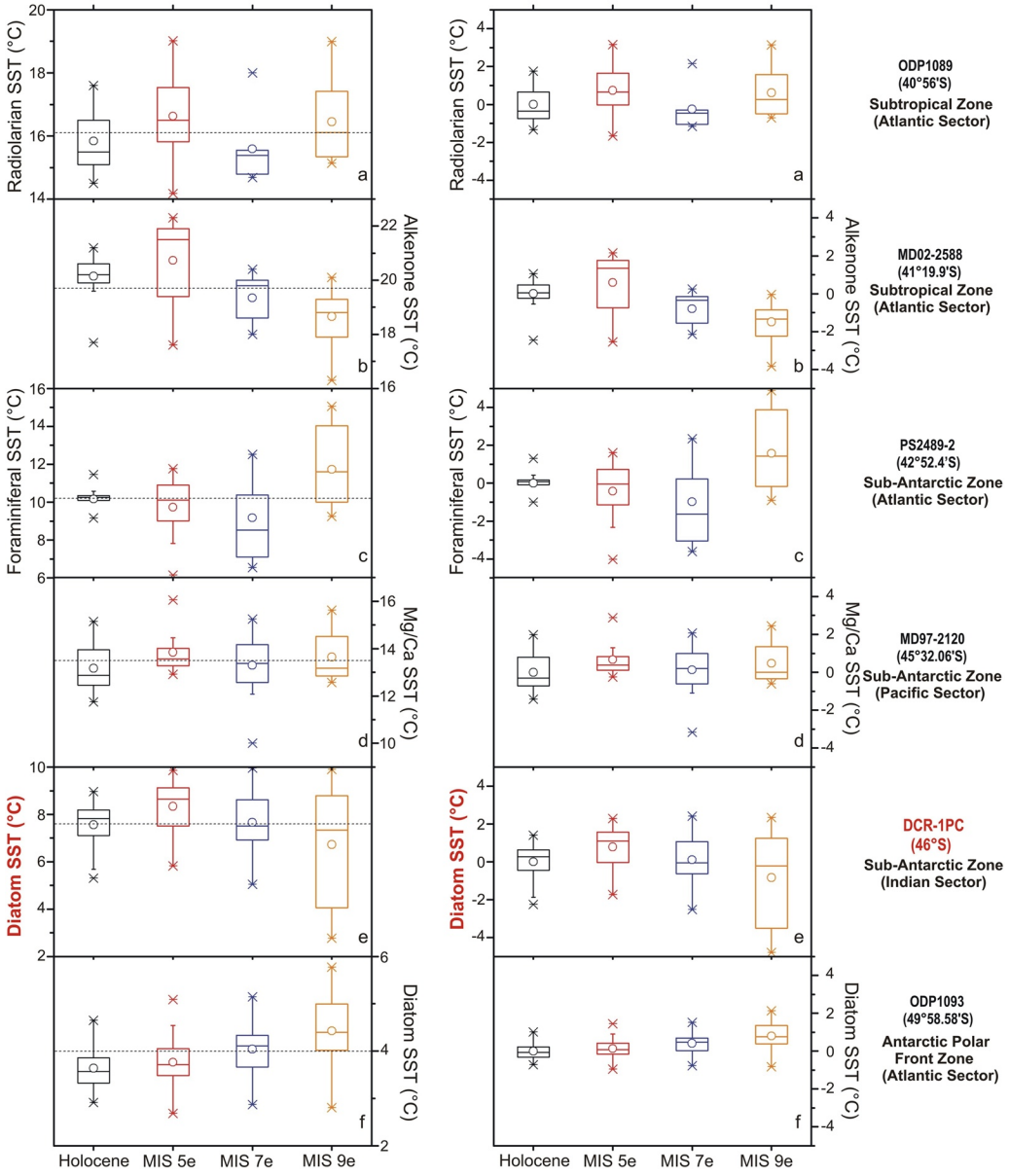

Figure 3. Box and whisker plots show SST variability during the past four IGs: the Holocene (0–11.7 ka), MIS 5e (~116–131 ka), MIS 7e (~234.7–247 ka), and MIS 9e (~324.8–338 ka). Left column: original values. Right column: anomalies relative to the Holocene values fixing at zero. The horizontal bar within each box represents the median value while the empty circle represents the mean value discussed in the text. The horizontal dash lines (left column) represent the mean SST averaged over the four IGs.

except in the Atlantic SAZ cores PS2489-2 and MD02-2588 in which mean SST was ~1°C lower in MIS 7e than in the Holocene (Figures 3b and 3c). Eventually, the hierarchy, as defined in core DCR-1PC, seems dependent on the strength of MIS 9e. A completely different ranking is observable in the APF core in which the mean SST of each IG decreased over the last 350 ka, with MIS 9e being significantly warmer and MIS 5e and the Holocene presenting almost similar mean SST (Figures 2f and 3f). Very close mean SST values during the MIS 5e and Holocene were also found in cores MD88-551 (Pichon et al., 1992) and PS58/271–1 (Esper & Gersonde, 2014) from the Indian and Pacific Permanent Open Ocean Zone, respectively. Globally, data compilations show MIS 5e to be the warmest IG of the last 350 ka (Lang & Wolff, 2011; Masson-Delmotte et al., 2010; PIWG, 2016; Shakun et al., 2015), with the highest sea level (Rohling et al., 2009) and most reduced ice-sheet (Lisiecki & Raymo, 2005). Conversely, insolation and CO_2-forced models documented MIS

9e, a time when atmospheric CO_2 concentrations were highest (Bereiter et al., 2015), as the warmest among the last four IGs (Yin & Berger, 2012), probably as a direct response to the CO_2 forcing.

The multi-millennial SST patterns in the SAZ cores generally show an early climate optimum and a drop in SST throughout a given IG (Figure 2). Conversely, the ODP Site 1093 record from the APF documents a pattern similar to the one observed in DCR-1PC for the three oldest IGs: two (early and late) warm phases interrupted by a cool phase (Figure 2). Such a pattern was also noticeable in the south Atlantic for the Holocene (Nielsen et al., 2004) and southwest Pacific for MIS 5e (Crosta et al., 2004). We, however, note that in core DCR-1PC, the first warming phase occurred at the end of the last deglaciation, and that the second warm phase was initiated at ~8 ka BP, during the early Holocene, and lasted until the late Holocene. These results suggest different climate dynamics in different latitudinal bands for the past four IGs. Such different response was previously observed for the Holocene (Denis et al., 2010; Lorenz et al., 2006) and attributed to precession and obliquity changes (Davis & Brewer, 2009), with the influence of obliquity sharply dropping north of ~43°S (Berger & Loutre, 1991).

In core DCR-1PC, the millennial-scale SST variability appears to be highest during MIS 9e and lowest during Holocene while MIS 5e and 7e experienced comparable intermediate variability (Figure 2e). Highest SST variability is similarly encountered in MIS 9e in most published marine records, except in core MD02-2588, in which SST were most variable during MIS 5e. Lowest SST variability is also similarly evidenced in most Holocene records, except in core MD97-2120, in which SST were least variable during MIS 5e (Figure 3d). Further detection of SST variability during different IGs is hampered by the lack of high-resolution records. We, however, note that most Holocene records show low SST variability (e.g., Anderson et al., 2009; Xiao et al., 2016 and references therein) and the few records that exist suggest higher SST variability during MIS 5e than during the Holocene (Crosta et al., 2004; Esper & Gersonde, 2014; Pichon et al., 1992). These results suggest lower climate variability during the Holocene compared to previous IGs in the SO. The few records available suggest that SST variability within each IG increases from south to north. Indeed, SST variability is ~1°C in APF core ODP1093, ~1–2°C in SAF core DCR-1PC (except MIS 9e), and ~2–3°C in SAZ cores (Figure 3).

3.3. Potential Drivers of SST over the Last Four Interglacial Periods

Models suggest that the strength of each IG over the last 800 ka is related to the magnitude of the forcing due to insolation and atmospheric CO_2 concentrations (Yin & Berger, 2012). However, feedbacks related to the AMOC, Antarctic sea-ice, and the Antarctic ice sheets (AIS) appear necessary to explain the full strength of past IGs. More precisely, melting of the NH ice-sheets reduced the formation of the North Atlantic Deep Water (NADW) (Govin et al., 2012), which reduced the northward heat transport and warmed the Southern Hemisphere (SH) as part of the bipolar seesaw (Holden et al., 2010; Masson-Delmotte et al., 2010). The SO warming induced Antarctic sea-ice retreat along with a more southern position of the SH Westerly Winds and SO hydrological fronts, which allowed for a more intense SO upwelling and, thus, CO_2 outgassing (Kohfeld et al., 2013). Comparing DCR-1PC SST with other SO SST records, NH summer insolation and CO_2 concentration, tends to support these hypotheses. Indeed, highest NH insolation and CO_2 concentration are found during the early MIS 5e when SO SST, Antarctic temperatures, and global sea-level were highest (Figure 4b). The very low sea-ice cover during the peak MIS 5e (Chadwick et al., 2020; Holloway et al., 2017), along with the prolonged weakened AMOC over Termination 2 (Deaney et al., 2017), may have allowed more heat to accumulate in the SO through the bipolar seesaw and more CO_2 to escape from SO deep waters to the atmosphere. Both processes provided a positive feedback on SO SST during the early MIS 5e. Similarly, somewhat higher mean SST during the early MIS 9e and 7e than during the early Holocene (11.7–8.5 ka) was congruent to higher NH insolation and CO_2 values (Figures 4a, 4c and 4d). We also note that no millennial variability is observed in EDC δD record over Termination 3 and 4 (Figures 4c and 4d). A weak/shallow AMOC is thus inferred by analogy to Termination 2, leading to a strong warming of SO waters during the early MIS 9e and 7e through the bipolar seesaw and CO_2 outgassing (Holden et al., 2010).

The short cool phase subsequent to the early IG warming (MIS 9e, 7e, and 5e in core DCR-1PC) is mainly attributed to feedback from the AIS. The warm SO during the early IG enhanced the AIS melting. This freshwater forcing increased the buoyancy of SO surface waters and reduced Antarctic Bottom water (AABW) formation, which subsequently cooled the SO and warmed the northern Atlantic through the bipolar

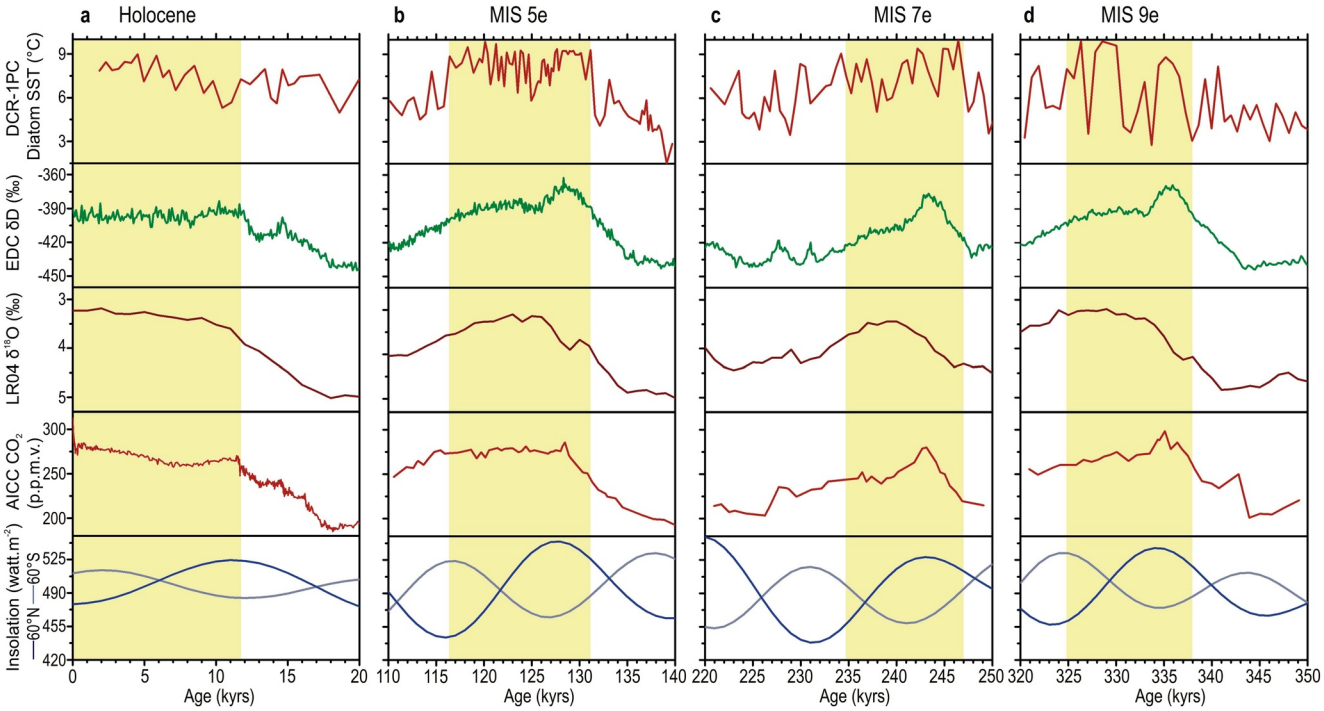

Figure 4. Comparison of core DCR-1PC SST (topmost red curve - this study) with past climatic records: EDC deuterium record (green curve - Bazin et al., 2013), $\delta^{18}O$ record of LR04 (brown curve–Lisiecki & Raymo, 2005), AICC CO_2 record (lower red curve - Bereiter et al., 2015), and summer insolation (Berger & Loutre, 1991) at 60°N (dark blue curve) and 60°S (light blue curve) for the past four terminations. Interglacials are highlighted in yellow.

seesaw (Bakker et al., 2017; Holden et al., 2010). A similar mechanism was proposed to explain the cooling of SO surface waters from 10–8 ka (Mathiot et al., 2013) and supports the early Holocene cooling observed in core DCR-1PC. However, another modeling study calls upon the resumption of upwelling of cold NADW in the SO due to the melting of Laurentide Ice Sheet, therefore counter-acting the bipolar seesaw (Renssen et al., 2010).

All IGs in core DCR-1PC present a late warming phase (Figure 2e), which cannot be driven by NH insolation that declined in all IGs over time (Figure 4). The late Holocene SST peak was related to the increasing influence of SH summer insolation (Nielsen et al., 2004), probably through snow-ice albedo feedback (Renssen et al., 2005). The warming caused by the increasing local insolation melted sea-ice. The newly ice-free areas of the SO absorbed more incoming solar radiation and enhanced the SO upwelling and, thus, CO_2 outgassing to the atmosphere (Studer et al., 2018), exerting positive feedback on SST. A similar switch between NH and SH summer insolation occurred during the mid-to-late part of all IGs, and in combination with CO_2, it may explain the strength of the second peak. Indeed, SST were high during the late MIS 9e, 5e, and the late Holocene when both SH summer insolation and CO_2 concentrations were high (Figures 4a, 4b, and 4d) while SST were low during the late MIS 7e when SH insolation and CO_2 concentration were lower than in other IGs (Figure 4c).

Multi-centennial to millennial climate variability during the Holocene has been attributed to changes in oceanic circulation (Debret et al., 2007; Latif et al., 2013; Mjell et al., 2015) and solar activity (Dima & Lohmann, 2009; Leventer et al., 1996). However, there might not be enough energy changes associated with solar variability to explain millennial SST variations of 2–4°C (Cubasch et al., 2006). The compilation of SST shows that the millennial variability was generally lesser during the Holocene than during previous IGs (Figure 2) in agreement with findings from the NH (Galaasen et al., 2020). Greater climate variability in older IGs was attributed to greater variability in NADW formation (Galaasen et al., 2014). However, a SO source of thermohaline circulation variability is also possible, whereby fluctuations in AABW production have been shown to induce far-field climate changes through the AMOC (Bakker et al., 2017). In the latter case, our results suggest that the variability in SO thermohaline circulation was generally greater during

IGs beyond the Holocene. It is possible that the smaller Antarctic sea-ice extent during MIS 5e than during the Holocene (Chadwick et al., 2020; Holloway et al., 2017) increased the sensitivity of SO upper and lower overturning cells to external and internal forcing (Parise et al., 2015), subsequently impacting the AMOC and global climate. To this goal, more high-resolution SST records covering different SO oceanographic realms are urgently needed.

4. Conclusions

We have presented the first high-resolution SST data covering the past four IGs from the sub-Antarctic region of the western Indian SO. Comparison of the new SST data with previous past climatic records allowed us to present a global framework of past climatic conditions in the SO. The new SST data reveal MIS 5e as the warmest IG of the past 350 ka, followed by similarly warm 9e, 7e, and Holocene. Each IG, except the Holocene, presents two warm phases (early and late), interrupted by a cooling. However, the duration of these phases within each IG is variable. We attribute both the strength and climate patterns to orbital configurations prevailing prior to and during each IG along with feedbacks from the NH and Antarctic ice-sheets, the AMOC and the carbon cycle. Our high-resolution record also allows us to document SST amplitude changes at the millennial timescale. The Holocene presents the lowest SST millennial variability amongst the past four IGs. These results suggest that millennial disruptions of the AMOC initiated either in the North Atlantic or in the SO, might have been larger during warmer-than-present conditions, thus suggesting possible disruption of the AMOC under future warming.

Data Availability Statement

Data are available at (Crosta & Shukla, 2020), https://doi.org/10.1594/PANGAEA.913651.

Acknowledgments
This work was funded by the institutional grant of the Birbal Sahni Institute of Palaeosciences (BSIP In-house Project No. 7.3 - BSIP/RDCC/29/2020–2021) to SKS for which BSIP Director is thanked. This work was also partially supported by SERB-OPDF to SKS visiting Xavier Crosta. Minoru Ikehara acknowledges the JSPS KAKENHI grant (No. JP19340156, JP23244102, JP17H06318). The authors thank chief scientist, Dr. Y. Nogi, NIPR, the captain, crew, and all researchers of Cruise KH10-07 onboard R/V Hakuho-Maru 2010. The authors also thank GRL editor Dr. Kathleen Donohue and four anonymous reviewers for their constructive comments.

References

Anderson, R. F., Ali, S., Bradtmiller, L. I., Nielsen, S. H. H., Fleisher, M. Q., Anderson, B. E., & Burckle, L. H. (2009). Wind-driven upwelling in the southern ocean and the deglacial rise in atmospheric CO_2. *Science*, *323*(5920), 1443–1448. https://doi.org/10.1126/science.1167441

Bakker, P., Clark, P. U., Golledge, N. R., Schmittner, A., & Weber, M. E. (2017). Centennial-scale Holocene climate variations amplified by Antarctic Ice Sheet discharge. *Nature*, *541*(7635), 72–76. https://doi.org/10.1038/nature20582

Bazin, L., Landais, A., Lemieux-Dudon, B., Toyé Mahamadou Kele, H., Veres, D., Parrenin, F., et al. (2013). An optimized multi-proxy, multi-site Antarctic ice and gas orbital chronology (AICC2012): 120-800 ka. *Climate of the Past*, *9*, 1715–1731. https://doi.org/10.5194/cp-9-1715-2013

Becquey, S., & Gersonde, R. (2003). A 0.55-Ma paleotemperature record from the Subantarctic zone: Implications for Antarctic circumpolar current development. *Paleoceanography*, *18*(1), 1014. https://doi.org/10.1029/2000pa000576

Bereiter, B., Eggleston, S., Schmitt, J., Nehrbass-Ahles, C., Stocker, T. F., Fischer, H., et al. (2015). Revision of the EPICA Dome C CO_2 record from 800 to 600 kyr before present. *Geophysical Research Letters*, *42*(2), 542–549. https://doi.org/10.1002/2014gl061957

Berger, A., & Loutre, M. F. (1991). Insolation values for the climate of the last 10 million years. *Quaternary Science Reviews*, *10*(4), 297–317. https://doi.org/10.1016/0277-3791(91)90033-Q

Bintanja, R., Van Oldenborgh, G. J., Drijfhout, S. S., Wouters, B., & Katsman, C. A. (2013). Important role for ocean warming and increased ice-shelf melt in Antarctic sea-ice expansion. *Nature Geoscience*, *6*(5), 376–379. https://doi.org/10.1038/ngeo1767

Bushinsky, S. M., Landschützer, P., Rödenbeck, C., Gray, A. R., Baker, D., Mazloff, M. R., et al. (2019). Reassessing southern ocean air-sea CO_2 flux estimates with the addition of biogeochemical float observations. *Global Biogeochemical Cycles*, *33*(11), 1370–1388. https://doi.org/10.1029/2019gb006176

Capron, E., Govin, A., Stone, E. J., Masson-Delmotte, V., Mulitza, S., Otto-Bliesner, B., et al. (2014). Temporal and spatial structure of multi-millennial temperature changes at high latitudes during the Last Interglacial. *Quaternary Science Reviews*, *103*, 116–133. https://doi.org/10.1016/j.quascirev.2014.08.018

Chadwick, M., Allen, C. S., Sime, L. C., & Hillenbrand, C. D. (2020). Analysing the timing of peak warming and minimum winter sea-ice extent in the Southern Ocean during MIS 5e. *Quaternary Science Reviews*, *229*, 106134. https://doi.org/10.1016/j.quascirev.2019.106134

Cortese, G., Abelmann, A., & Gersonde, R. (2007). The last five glacial-interglacial transitions: A high-resolution 450,000-year record from the subantarctic Atlantic. *Paleoceanography*, *22*(4), PA4203. https://doi.org/10.1029/2007pa001457

Crosta, X., & Koç, N. (2007). Chapter eight diatoms: From micropaleontology to isotope geochemistry. *Developments in Marine Geology*, *1*, 327–369. https://doi.org/10.1016/s1572-5480(07)01013-5

Crosta, X., & Shukla, S. (2020). Sea surface temperatures of sediment core DCR-1PC. PANGAEA. https://doi.org/10.1594/PANGAEA.913651

Crosta, X., Shukla, S. K., Ther, O., Ikehara, M., Yamane, M., & Yokoyama, Y. (2020). Last abundant appearance datum of *Hemidiscus karstenii* driven by climate change. *Marine Micropaleontology*, *157*, 101861. https://doi.org/10.1016/j.marmicro.2020.101861

Crosta, X., Sturm, A., Armand, L., & Pichon, J.-J. (2004). Late Quaternary sea ice history in the Indian sector of the Southern Ocean as recorded by diatom assemblages. *Marine Micropaleontology*, *50*(3), 209–223. https://doi.org/10.1016/S0377-8398(03)00072-0

Cubasch, U., Zorita, E., Kaspar, F., Gonzalez-Rouco, J. F., Storch, H. v., & Prömmel, K. (2006). Simulation of the role of solar and orbital forcing on climate. *Advances in Space Research*, *37*(8), 1629–1634. https://doi.org/10.1016/j.asr.2005.04.076

Davis, B. A. S., & Brewer, S. (2009). Orbital forcing and role of the latitudinal insolation/temperature gradient. *Climate Dynamics*, *32*(2), 143–165. https://doi.org/10.1007/s00382-008-0480-9

Deaney, E. L., Barker, S., & van de Flierdt, T. (2017). Timing and nature of AMOC recovery across Termination 2 and magnitude of deglacial CO_2 change. *Nature Communications*, *8*(1), 14595. https://doi.org/10.1038/ncomms14595

Debret, M., Bout-Roumazeilles, V., Grousset, F., Desmet, M., McManus, J. F., Massei, N., et al. (2007). The origin of the 1500-year climate cycles in Holocene North-Atlantic records. *Climate of the Past*, *3*, 569–575. https://doi.org/10.5194/cp-3-569-2007

Denis, D., Crosta, X., Barbara, L., Massé, G., Renssen, H., Ther, O., & Giraudeau, J. (2010). Sea ice and wind variability during the Holocene in East Antarctica: Insight on middle-high latitude coupling. *Quaternary Science Reviews*, *29*(27), 3709–3719. https://doi.org/10.1016/j.quascirev.2010.08.007

Dima, M., & Lohmann, G. (2009). Conceptual model for millennial climate variability: A possible combined solar-thermohaline circulation origin for the ~1,500-year cycle. *Climate Dynamics*, *32*(2), 301–311. https://doi.org/10.1007/s00382-008-0471-x

Doddridge, E. W., Marshall, J., Song, H., Campin, J. M., Kelley, M., & Nazarenko, L. (2019). Eddy compensation dampens Southern Ocean sea surface temperature response to westerly wind trends. *Geophysical Research Letters*, *46*(8), 4365–4377. https://doi.org/10.1029/2019gl082758

Esper, O., & Gersonde, R. (2014). Quaternary surface water temperature estimations: New diatom transfer functions for the Southern Ocean. *Palaeogeography, Palaeoclimatology, Palaeoecology*, *414*, 1–19. https://doi.org/10.1016/j.palaeo.2014.08.008

Galaasen, E. V., Ninnemann, U. S., Irvali, N., Kleiven, H. F., Rosenthal, Y., Kissel, C., & Hodell, D. A. (2014). Rapid reductions in North Atlantic Deep Water during the peak of the last interglacial period. *Science*, *343*(6175), 1129–1132. https://doi.org/10.1126/science.1248667

Galaasen, E. V., Ninnemann, U. S., Kessler, A., Irvali, N., Rosenthal, Y., Tjiputra, J., et al. (2020). Interglacial instability of North Atlantic Deep Water ventilation. *Science*, *367*(6485), 1485–1489. https://doi.org/10.1126/science.aay6381

Golledge, N. R., Kowalewski, D. E., Naish, T. R., Levy, R. H., Fogwill, C. J., & Gasson, E. G. W. (2015). The multi-millennial Antarctic commitment to future sea-level rise. *Nature*, *526*(7573), 421–425. https://doi.org/10.1038/nature15706

Govin, A., Braconnot, P., Capron, E., Cortijo, E., Duplessy, J.-C., Jansen, E., et al. (2012). Persistent influence of ice sheet melting on high northern latitude climate during the early Last Interglacial. *Climate of the Past*, *8*, 483–507. https://doi.org/10.5194/cp-8-483-2012

Govin, A., Michel, E., Labeyrie, L., Waelbroeck, C., Dewilde, F., & Jansen, E. (2009). Evidence for northward expansion of Antarctic Bottom Water mass in the Southern Ocean during the last glacial inception. *Paleoceanography*, *24*(1), PA1202. https://doi.org/10.1029/2008pa001603

Hays, J. D., Imbrie, J., & Shackleton, N. J. (1976). Variations in the Earth's Orbit: Pacemaker of the ice ages. *Science*, *194*(4270), 1121–1132. https://doi.org/10.1126/science.194.4270.1121

Ho, S. L., Mollenhauer, G., Lamy, F., Martínez-Garcia, A., Mohtadi, M., Gersonde, R., et al. (2012). Sea surface temperature variability in the Pacific sector of the Southern Ocean over the past 700 kyr. *Paleoceanography*, *27*(4), PA4202. https://doi.org/10.1029/2012pa002317

Holden, P. B., Edwards, N. R., Wolff, E. W., Lang, N. J., Singarayer, J. S., Valdes, P. J., & Stocker, T. F. (2010). Interhemispheric coupling, the West Antarctic Ice Sheet and warm Antarctic interglacials. *Climate of the Past*, *6*(4), 431–443. https://www.clim-past.net/6/431/2010/

Holloway, M. D., Sime, L. C., Allen, C. S., Hillenbrand, C.-D., Bunch, P., Wolff, E., & Valdes, P. J. (2017). The spatial structure of the 128 ka Antarctic Sea ice minimum. *Geophysical Research Letters*, *44*(21), 11129–11139. https://doi.org/10.1002/2017gl074594

Howard, W. R., & Prell, W. L. (1992). Late Quaternary surface circulation of the southern Indian Ocean and its relationship to orbital variations. *Paleoceanography*, *7*(1), 79–117. https://doi.org/10.1029/91pa02994

Ikehara, M., Kawamura, K., Ohkouchi, N., Kimoto, K., Murayama, M., Nakamura, T., et al. (1997). Alkenone sea surface temperature in the Southern Ocean for the last two deglaciations. *Geophysical Research Letters*, *24*(6), 679–682. https://doi.org/10.1029/97gl00429

Jones, J. M., Gille, S. T., Goosse, H., Abram, N. J., Canziani, P. O., Charman, D. J., et al. (2016). Assessing recent trends in high-latitude Southern Hemisphere surface climate. *Nature Climate Change*, *6*(10), 917–926. https://doi.org/10.1038/nclimate3103

Jouzel, J., Masson-Delmotte, V., Cattani, O., Dreyfus, G., Falourd, S., Hoffmann, G., et al. (2007). Orbital and millennial Antarctic climate variability over the past 800,000 years. *Science*, *317*(5839), 793–796. https://doi.org/10.1126/science.1141038

Kohfeld, K. E., Graham, R. M., De Boer, A. M., Sime, L. C., Wolff, E. W., Le Quéré, C., & Bopp, L. (2013). Southern Hemisphere westerly wind changes during the Last Glacial Maximum: Paleo-data synthesis. *Quaternary Science Reviews*, *68*, 76–95. https://doi.org/10.1016/j.quascirev.2013.01.017

Labeyrie, L., Labracherie, M., Gorfti, N., Pichon, J. J., Vautravers, M., Arnold, M., et al. (1996). Hydrographic changes of the Southern Ocean (southeast Indian sector) over the last 230 kyr. *Paleoceanography*, *11*(1), 57–76. https://doi.org/10.1029/95pa02255

Lang, N., & Wolff, E. W. (2011). Interglacial and glacial variability from the last 800 ka in marine, ice and terrestrial archives. *Climate of the Past*, *7*, 361–380. https://doi.org/10.5194/cp-7-361-2011

Latif, M., Martin, T., & Park, W. (2013). Southern Ocean sector centennial climate variability and recent decadal trends. *Journal of Climate*, *26*(19), 7767–7782. https://doi.org/10.1175/JCLI-D-12-00281.1

Le Quéré, C., Andrew, R. M., Friedlingstein, P., Sitch, S., Hauck, J., Pongratz, J., et al. (2018). Global carbon budget 2018. *Earth System Science Data*, *10*(4), 2141–2194. https://doi.org/10.5194/essd-10-2141-2018

Lefebvre, W., & Goosse, H. (2008). An analysis of the atmospheric processes driving the large-scale winter sea ice variability in the Southern Ocean. *Journal of Geophysical Research*, *113*(C2), C02004. https://doi.org/10.1029/2006jc004032

Leventer, A., Domack, E. W., Ishman, S. E., Brachfeld, S., McClennen, C. E., & Manley, P. (1996). Productivity cycles of 200-300 years in the Antarctic Peninsula region: Understanding linkages among the sun, atmosphere, oceans, sea ice, and biota. *GSA Bulletin*, *108*(12), 1626–1644. https://doi.org/10.1130/0016-7606(1996)108<1626:PCOYIT>2.3.CO;2

Lisiecki, L. E., & Raymo, M. E. (2005). A Pliocene-Pleistocene stack of 57 globally distributed benthic $\delta^{18}O$ records. *Paleoceanography*, *20*(1), PA1003. https://doi.org/10.1029/2004pa001071

Locarnini, R. A., Mishonov, A. V., Antonov, J. I., Boyer, T. P., Garcia, H. E., Baranova, O. K., et al. (2013). World ocean atlas 2013 (Volume 1. Temperature). Atlas. Retrieved from https://repository.library.noaa.gov/view/noaa/14847

Lorenz, S. J., Kim, J. H., Rimbu, N., Schneider, R. R., & Lohmann, G. (2006). Orbitally driven insolation forcing on Holocene climate trends: Evidence from alkenone data and climate modeling. *Paleoceanography*, *21*(1), PA1002. https://doi.org/10.1029/2005pa001152

Marshall, J., & Speer, K. (2012). Closure of the meridional overturning circulation through Southern Ocean upwelling. *Nature Geoscience*, *5*(3), 171–180. https://doi.org/10.1038/ngeo1391

Martínez-Garcia, A., Rosell-Melé, A., Geibert, W., Gersonde, R., Masqué, P., Gaspari, V., & Barbante, C. (2009). Links between iron supply, marine productivity, sea surface temperature, and CO_2 over the last 1.1 Ma. *Paleoceanography*, *24*(1), PA1207. https://doi.org/10.1029/2008PA001657

Masson-Delmotte, V., Stenni, B., Pol, K., Braconnot, P., Cattani, O., Falourd, S., et al. (2010). EPICA Dome C record of glacial and interglacial intensities. *Quaternary Science Reviews*, *29*(1), 113–128. https://doi.org/10.1016/j.quascirev.2009.09.030

Mathiot, P., Goosse, H., Crosta, X., Stenni, B., Braida, M., Renssen, H., et al. (2013). Using data assimilation to investigate the causes of Southern Hemisphere high latitude cooling from 10 to 8 ka BP. *Climate of the Past*, *9*(2), 887–901. https://doi.org/10.5194/cp-9-887-2013

Mjell, T. L., Ninnemann, U. S., Eldevik, T., & Kleiven, H. K. F. (2015). Holocene multidecadal- to millennial-scale variations in Iceland-Scotland overflow and their relationship to climate. *Paleoceanography*, *30*(5), 558–569. https://doi.org/10.1002/2014pa002737

Nielsen, S. H. H., Koç, N., & Crosta, X. (2004). Holocene climate in the Atlantic sector of the Southern Ocean: Controlled by insolation or oceanic circulation? *Geology*, *32*(4), 317–320. https://doi.org/10.1130/G20334.1

Orsi, A. H., Whitworth, T., & Nowlin, W. D. (1995). On the meridional extent and fronts of the Antarctic Circumpolar Current. *Deep Sea Research I: Oceanographic Research Papers*, *42*(5), 641–673. https://doi.org/10.1016/0967-0637(95)00021-w

Pahnke, K., Zahn, R., Elderfield, H., & Schulz, M. (2003). 340,000-year centennial-scale marine record of Southern Hemisphere climatic oscillation. *Science*, *301*(5635), 948–952. https://doi.org/10.1126/science.1084451

Parise, C. K., Pezzi, L. P., Hodges, K. I., & Justino, F. (2015). The influence of sea ice dynamics on the climate sensitivity and memory to increased Antarctic Sea Ice. *Journal of Climate*, *28*(24), 9642–9668. https://doi.org/10.1175/JCLI-D-14-00748.1

Past Interglacials Working Group of PAGES. (2016). Interglacials of the last 800,000 years. *Reviews of Geophysics*, *54*, 162–219. https://doi.org/10.1002/2015RG000482

Pauling, A. G., Smith, I. J., Langhorne, P. J., & Bitz, C. M. (2017). Time-dependent freshwater input from ice shelves: Impacts on Antarctic Sea Ice and the Southern Ocean in an Earth system model. *Geophysical Research Letters*, *44*(20), 10454–10461. https://doi.org/10.1002/2017gl075017

Pichon, J.-J., Labeyrie, L. D., Bareille, G., Labracherie, M., Duprat, J., & Jouzel, J. (1992). Surface water temperature changes in the high latitudes of the southern hemisphere over the Last Glacial-Interglacial Cycle. *Paleoceanography*, *7*(3), 289–318. https://doi.org/10.1029/92pa00709

Pollard, R., Venables, H., Read, J., & Allen, J. (2007). Large-scale circulation around the Crozet Plateau controls an annual phytoplankton bloom in the Crozet Basin. *Deep Sea Research Part II: Topical Studies in Oceanography*, *54*(18–20), 1915–1929. https://doi.org/10.1016/j.dsr2.2007.06.012

Rahmstorf, S., Box, J. E., Feulner, G., Mann, M. E., Robinson, A., Rutherford, S., & Schaffernicht, E. J. (2015). Exceptional twentieth-century slowdown in Atlantic Ocean overturning circulation. *Nature Climate Change*, *5*(5), 475–480. https://doi.org/10.1038/nclimate2554

Renssen, H., Goosse, H., Crosta, X., & Roche, D. M. (2010). Early Holocene Laurentide Ice Sheet deglaciation causes cooling in the high-latitude Southern Hemisphere through oceanic teleconnection. *Paleoceanography*, *25*(3), PA3204. https://doi.org/10.1029/2009pa001854

Renssen, H., Goosse, H., Fichefet, T., Masson-Delmotte, V., & Koç, N. (2005). Holocene climate evolution in the high-latitude Southern Hemisphere simulated by a coupled atmosphere-sea ice-ocean-vegetation model. *The Holocene*, *15*(7), 951–964. https://doi.org/10.1191/0959683605hl869ra

Rignot, E., Mouginot, J., Scheuchl, B., van den Broeke, M., van Wessem, M. J., & Morlighem, M. (2019). Four decades of Antarctic Ice Sheet mass balance from 1979-2017. *Proceedings of the National Academy of Sciences of the United States of America*, *116*(4), 1095–1103. https://doi.org/10.1073/pnas.1812883116

Rintoul, S. R. (2018). The global influence of localized dynamics in the Southern Ocean. *Nature*, *558*(7709), 209–218. https://doi.org/10.1038/s41586-018-0182-3

Rohling, E. J., Grant, K., Bolshaw, M., Roberts, A. P., Siddall, M., Hemleben, C., & Kucera, M. (2009). Antarctic temperature and global sea level closely coupled over the past five glacial cycles. *Nature Geoscience*, *2*(7), 500–504. https://doi.org/10.1038/ngeo557

Romero, O. E., Kim, J.-H., Bárcena, M. A., Hall, I. R., Zahn, R., & Schneider, R. (2015). High-latitude forcing of diatom productivity in the southern Agulhas Plateau during the past 350 kyr. *Paleoceanography*, *30*(2), 118–132. https://doi.org/10.1002/2014pa002636

Schneider-Mor, A., Yam, R., Bianchi, C., Kunz-Pirrung, M., Gersonde, R., & Shemesh, A. (2008). Nutrient regime at the siliceous belt of the Atlantic sector of the Southern Ocean during the past 660 ka. *Paleoceanography*, *23*(3), PA3217. https://doi.org/10.1029/2007PA001466

Shakun, J., Clark, P., He, F., et al. (2015). Regional and global forcing of glacier retreat during the last deglaciation. *Nature Communications*, *6*, 8059. https://doi.org/10.1038/ncomms9059

Shin, S. I., Liu, Z., Otto-Bliesner, B. L., Kutzbach, J. E., & Vavrus, S. J. (2003). Southern Ocean sea-ice control of the glacial North Atlantic thermohaline circulation. *Geophysical Research Letters*, *30*(2), 1096. https://doi.org/10.1029/2002gl015513

Sokolov, S., & Rintoul, S. R. (2009). Circumpolar structure and distribution of the Antarctic Circumpolar Current fronts: 1. Mean circumpolar paths. *Journal of Geophysical Research*, *114*(C11). https://doi.org/10.1029/2008jc005108

Studer, A. S., Sigman, D. M., Martínez-García, A., Thöle, L. M., Michel, E., Jaccard, S. L., et al. (2018). Increased nutrient supply to the Southern Ocean during the Holocene and its implications for the pre-industrial atmospheric CO_2 rise. *Nature Geoscience*, *11*(10), 756–760. https://doi.org/10.1038/s41561-018-0191-8

Swingedouw, D., Fichefet, T., Huybrechts, P., Goosse, H., Driesschaert, E., & Loutre, M. F. (2008). Antarctic ice-sheet melting provides negative feedbacks on future climate warming. *Geophysical Research Letters*, *35*(17), L17705. https://doi.org/10.1029/2008gl034410

Timmermann, R., & Hellmer, H. H. (2013). Southern Ocean warming and increased ice shelf basal melting in the twenty-first and twenty-second centuries based on coupled ice-ocean finite-element modelling. *Ocean Dynamics*, *63*(9–10), 1011–1026. https://doi.org/10.1007/s10236-013-0642-0

Waelbroeck, C., Jouzel, J., Labeyrie, L., Lorius, C., Labracherie, M., Stiévenard, M., & Barkov, N. I. (1995). A comparison of the Vostok ice deuterium record and series from Southern Ocean core MD 88-770 over the last two glacial-interglacial cycles. *Climate Dynamics*, *12*(2), 113–123. https://doi.org/10.1007/BF00223724

Xiao, W., Esper, O., & Gersonde, R. (2016). Last Glacial - Holocene climate variability in the Atlantic sector of the Southern Ocean. *Quaternary Science Reviews*, *135*, 115–137. https://doi.org/10.1016/j.quascirev.2016.01.023

Yin, Q. (2013). Insolation-induced mid-Brunhes transition in Southern Ocean ventilation and deep-ocean temperature. *Nature*, *494*, 222–225. https://doi.org/10.1038/nature11790

Yin, Q. Z., & Berger, A. (2012). Individual contribution of insolation and CO_2 to the interglacial climates of the past 800,000 years. *Climate Dynamics*, *38*, 709–724. https://doi.org/10.1007/s00382-011-1013-5

References From the Supporting Information

Becquey, S., & Gersonde, R. (2002). Past hydrographic and climatic changes in the subantarctic Zone of the South Atlantic - The Pleistocene record from ODP Site 1090. *Palaeogeography, Palaeoclimatology, Palaeoecology*, *182*(3), 221–239. https://doi.org/10.1016/s0031-0182(01)00497-7

Cortese, G., & Abelmann, A. (2002). Radiolarian-based paleotemperatures during the last 160 kyr at ODP Site 1089 (Southern Ocean, Atlantic Sector). *Palaeogeography, Palaeoclimatology, Palaeoecology*, *182*(3), 259–286. https://doi.org/10.1016/s0031-0182(01)00499-0

Crosta, X., Pichon, J.-J., & Burckle, L. H. (1998). Application of modern analog technique to marine Antarctic diatoms: Reconstruction of maximum sea-ice extent at the Last Glacial Maximum. *Paleoceanography*, *13*(3), 284–297. https://doi.org/10.1029/98pa00339

Mashiotta, T. A., Lea, D. W., & Spero, H. J. (1999). Glacial-interglacial changes in Subantarctic sea surface temperature and δ18O-water using foraminiferal Mg. *Earth and Planetary Science Letters*, *170*(4), 417–432. https://doi.org/10.1016/s0012-821x(99)00116-8

Prahl, F., Herbert, T., Brassell, S. C., Ohkouchi, N., Pagani, M., Repeta, D., et al. (2000). Status of alkenone paleothermometer calibration: Report from Working Group 3. *Geochemistry, Geophysics, Geosystems*, *1*(11), 1034. https://doi.org/10.1029/2000gc000058

Sikes, E. L., Volkman, J. K., Robertson, L. G., & Pichon, J.-J. (1997). Alkenones and alkenes in surface waters and sediments of the Southern Ocean: Implications for paleotemperature estimation in polar regions. *Geochimica et Cosmochimica Acta*, *61*(7), 1495–1505. https://doi.org/10.1016/s0016-7037(97)00017-3